

# Effectiveness of an Eco-friendly Polymer Composite Sand-Fixing Agent on Sand Fixation

Guofu Ma · Feitian Ran · Enke Feng · Zhibao Dong ·  
Ziqiang Lei

Received: 22 March 2015 / Accepted: 4 June 2015  
© Springer International Publishing Switzerland 2015

**Abstract** A novel and eco-friendly xanthan gum-g-poly(acrylic acid)/laterite (XG-g-PAA/laterite) organic-inorganic composite polymer used as chemical sand-fixing agent (CSFA) was successfully prepared by grafted copolymerization of natural XG, partially neutralized acrylic acid (NaA), and laterite in solution. FTIR spectra confirmed that NaA had been grafted onto XG chains, and the –OH groups of laterite participated in polymerization reaction. The influence of the content of CSFA on sand-fixing effect was investigated, and the results of the aging test indicated that the CSFA had remarkable water resistance, heat resistance, anti-freeze-thaw, and anti-ultraviolet aging performances, which could meet the requirement of application in the harsh desert environment. Moreover, it also showed excellent water-retaining and anti-evaporation properties.

**Keywords** Sand-fixing agent · Xanthan gum · Laterite · Compressive strength

## 1 Introduction

Desertification has long been recognized as a major economic, social, and environmental problem of concern to many countries in all regions of the world (Jiang et al. 2014). China is one of several countries severely affected by desertification (Wang et al. 2002). The land desertification of China accounts for 27.3 % of the total land area according to the first national survey on desertification land. Approximately 99.6 % of this land is distributed in 12 provinces or autonomous regions in north and northwest China. A recent survey has shown that over 90 % of grassland in north China suffered from different degrees of degradation and that degradation rate reached 6700 km<sup>2</sup> per year (Zhou et al. 2015). Desertification leads to fragmented ecosystem structure and decreased carbon storage (Asner and Martin 2004) and jeopardizes the livelihoods of nearly 200 million people as well as has a significant impact on the subsistence of historical populations (Hua et al. 2014; Wang et al. 2008a, b). Multiple desertification cycles that occurred in these regions (Dong et al. 1995; Wang et al. 2010) affect the livelihoods of inhabitants, impact the prosperity, and lead to the abandonment of ancient cities (Wang and Dong 2001). Therefore, controlling and combating desertification in China is one of great and far-reaching significance (Musa et al. 2014).

---

G. Ma (✉) · F. Ran · E. Feng · Z. Lei (✉)  
Key Laboratory of Eco-Environment-Related Polymer  
Materials, Ministry of Education, Key Laboratory of Polymer  
Materials of Gansu Province, Northwest Normal University,  
Lanzhou 730070, China  
e-mail: magf@nwnu.edu.cn  
e-mail: leizq@nwnu.edu.cn

G. Ma · Z. Dong  
Cold and Arid Regions Environmental and Engineering  
Research Institute, Chinese Academy of Sciences,  
Lanzhou 730070, China

Many strategies have been made to combat desertification, including better preservation of original dry land ecosystems and desert restoration. In desert restoration, sand fixation materials are usually employed to immobilize sand dunes and provide an environment for seed germination (Duan et al. 2014). However, the traditional sand fixation materials including physical barriers (e.g., gravel (Li et al. 2000), straw (Ji and Unger 2001)), petroleum heavy oil and asphalt emulsions (Hashemianesh and Matinfar 2012; Asi et al. 2002), and biological soil crust (e.g., lichen (Eldridge and Ferris 1999), cyanobacteria (Mazor et al. 1996)) have their own limitations in terms of costs, effectiveness, and convenience in implementation. Therefore, novel chemical materials, which can prevent wind erosion, maintaining the water and improving the nature of the sand, have gained much attention.

An ideal chemical sand-fixing agent should have benefits such as low cost, easy to produce and apply, able to form a high erosion resistance crust, and no additional pollution to the environment (Dong et al. 2008). Recently, organic polymerized materials which can produce a crust on loose sand surface to increase sand aggregate stability, reduce water evaporation, and improve anti-wind erosion ability have received much attention. However, most of the organic polymerized materials that have been developed do not have a high erosion resistance crust and water-retaining capacity (Liu et al. 2012).

In this work, a novel, cost-effective, and eco-friendly xanthan gum-g-poly(acrylic acid)/laterite (XG-g-PAA/laterite) organic-inorganic composite polymer used as a chemical sand-fixing agent (CSFA) was successfully prepared. The introduction of XG-g-PAA/laterite was expected to provide a new way to extend the utilization of laterite and, more specifically, to lower the cost of production and improve the biocompatibility and biodegradability of the CSFA. The composite polymer was characterized by Fourier transform infrared (FTIR) spectroscopy, X-ray diffraction (XRD), thermogravimetry (TG/TGA), and element mapping. The cross-sectional structure of the sand fixation specimens was characterized by scanning electron microscopy (SEM), and the influence of the content of CSFA on sand-fixing effect was also investigated. To understand the sand-fixing effect of XG-g-PAA/laterite, performance tests of specimens including water resistance, thermal aging, freeze-thaw aging, ultraviolet (UV)

radiation aging, and water retention were performed systematically in the laboratory.

## 2 Experiment

### 2.1 Materials

The following materials were used in the study: laterite (collected from WuQuan Mountain in Lanzhou City, Gansu Province, China), XG (analytical grade, from Tianjin Guangfu Institute of Fine Chemicals, China), acrylic acid (AA, analytical grade, from Tianjian Kaixin Chemical Industrial Co., China), ammonium persulfate (APS, analytical grade, from Yantai Shuangshuang Chemical Industrial Co., China), and *N,N*-methylenebisacrylamide (MBA, chemically pure, from Sinopharm Chemical Reagent Co., China). A sand sample was taken from Tengger Desert, Gansu Province, China. All the other reagents used were of analytical grade and all solutions were prepared with distilled water.

### 2.2 Texture of Experimental Sand

The texture analysis of the experimental sand with a maximum grain size of 0.3 mm used for this study is presented in Table 1. The dominant components of the sand were particle sizes between 0.10–0.15 and 0.15–0.20 mm.

### 2.3 Preparation of XG-g-PAA/Laterite Composite Sand-Fixing Agent

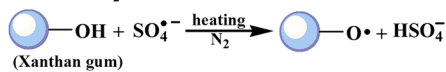
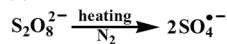
The general procedure adopted for the synthesis of XG-g-PAA/laterite composite sand-fixing agent is presented in Scheme 1. The synthesis was performed by the following steps:

**Table 1** Texture of experimental sand (in weight percent)

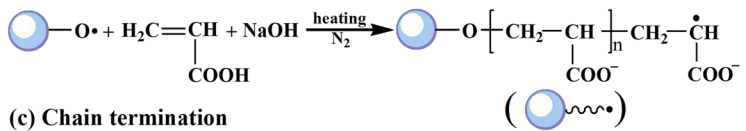
Grain size distribution (mm)			
>0.20	0.15–0.20	0.10–0.15	<0.10
4.64	48.20	44.35	2.81

**Scheme 1** Proposed reaction mechanism for preparation of XG-g-PAA/laterite sand-fixing agent

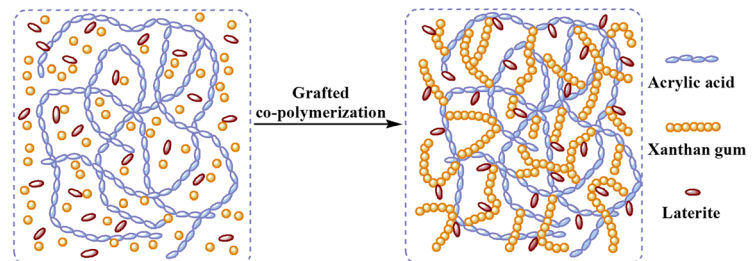
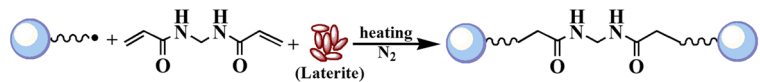
**(a) Chain initiation**



**(b) Chain propagation**



**(c) Chain termination**



### 2.3.1 Step 1. Laterite Purification

Natural laterite was found to contain small amounts of mineral impurities and the laterite was purified by the suspension method. A purification process was carried out by preparing a 10-wt% aqueous suspension of the laterite and allowing the more dense impurities, quartz and carbonates, to sediment out. After a certain sedimentation time, the supernatant suspension that is pure laterite was decanted off, and then the pure laterite was collected by filtration, dried, ground, and sieved. After that, the pure laterite with particle sizes about 0.074 mm (200 mesh) was obtained for further use.

### 2.3.2 Step 2. Preparation of XG-g-PAA/Laterite

XG-g-PAA/laterite was synthesized by the graft copolymerization reaction of AA, XG, and laterite in the presence of MBA as a cross-linking agent and APS as a free radical initiator. Typically, XG (1.2 g) was dissolved in 30.0 mL of distilled water in a three-neck flask equipped with a mechanical stirrer, a reflux condenser, and a nitrogen line at 70 °C for 1 h, and a transparent sticky solution was obtained. Then, 5 mL containing 0.1 g APS aqueous solution was added to the sticky solution and continuously stirred at 70 °C for 15 min to generate radicals. A 7.2-g AA was neutralized by

8.5 mL, 8.0 mol/L NaOH solution to obtain neutralized acrylic acid with neutralization degree of 70 % and fully mixed with 30 mg MBA and 0.95 g of laterite powder under magnetic stirring. After cooling the reactants to 50 °C, the mixture was added to the flask. The temperature was slowly increased to 70 °C and maintained for 3 h to complete the graft copolymerization reaction. A nitrogen atmosphere was maintained throughout the reaction period. The obtained products were dried in an oven at 60 °C to constant weight. Finally, the dried products were milled and screened. All of the samples used for the tests had a particle size of less than 150 μm (100 mesh) in diameter.

### 2.4 Preparation of Sand Fixation Specimens

The specimens mixed with different concentrations of CSFA were prepared as follows: a certain amount of sand, CSFA (0.4, 0.8, 1.2, 1.6, and 2 %, based on sand weight), and tap water (20 %, based on sand weight) were mixed to form a homogeneous mixture. The mixture was put into a mold (0.5 cm in height and 4 cm in diameter) and pressed tightly. Then the specimens were placed in an oven at 80 °C for 24 h until the sand particles are bonded together and the cementing sand was formed. The appearance of the sand fixation specimens containing 2 % CSFA is shown in Fig. 1.



**Fig. 1** The appearance of the sand fixation specimen containing 2 % CSFA (based on sand weight)

### 2.5 Compressive Strength Test

Compressive strength is an important parameter that is used to evaluate the sand-fixing property. Its measurement was carried out on a press machine (purchased from Cangzhou Jilu Test Instrument Co., China) and was measured as follows: the strength was loaded on the center of the sample until cracks appeared and the value was recorded as compressive strength.

### 2.6 Water Resistance Test

The specimens with different amounts of CSFA (0.4, 0.8, 1.6 %) were placed into the bottom of 250 mL beakers, and 50 mL tap water was poured into each container. Then they were put onto a table for 8 days under a room temperature environment. For the purpose of comparison, another group of specimens with different amounts of CSFA (0.4, 0.8, 1.6 %) were put into the  $\text{CaCl}_2$  solution with 10 wt% and immersed for 4 h. Then the specimens were taken out and placed in an oven at 80 °C for 24 h until they were dried completely. Other operations were the same as the above description.

### 2.7 Simulation of the Aging Test

Thermal aging, freeze-thaw aging, and UV irradiation aging were used to simulate the possible desert conditions. In the thermal test, the specimen was subjected to oxidation in a circulation oven at 80 °C for 24 days, while in the freeze-thaw cycle, the conditions were 22 h of freezing at -25 °C and 2 h of thawing at 25 °C, and the freeze-thaw test contained 20 cycles. In the UV radiation, the specimen was placed 20 cm under a 20-W ultraviolet lamp for 480 h at 25 °C. The compressive

strength changes of the sand fixation specimens were measured after different aging cycles, and all the aging tests were carried out continuously and there was no interruption in the whole process.

### 2.8 Water-Retaining Property

The water-retaining property was designed as follows: sand (120 g) that was mixed with a different amount of agent was filled into a plastic container with 58 mm in diameter and 85 mm in height. Then 40 g tap water was poured into each container. All containers were placed in an oven at 25 °C. The water-retaining property of each sand fixation specimen was determined every 1 day, and WR was calculated by the following equation:

$$\text{WR} = \frac{W - W_d}{W_0 - W_d} \times 100\%$$

where  $W_0$  is the weight of the original sand fixation specimen containing tap water,  $W_d$  is the weight of the dry sand fixation specimen, and  $W$  is the weight of the sand fixation specimen containing tap water placed for different times at 25 °C.

### 2.9 Characterization

FTIR measurements were performed on a FTIR-FTS3000 spectrometer. The samples were completely dried before measurement. All spectra where 40 scans over a wavenumber of 400–4000  $\text{cm}^{-1}$  at 8  $\text{cm}^{-1}$  resolution were collected were obtained from compressed KBr pellets in which the concentration of the samples was about 3 %. The morphologies of the sand fixation

specimen were examined using a field emission scanning electron microscope (FESEM, Carl Zeiss Ultra Plus, Germany) with an acceleration voltage of 3 kV. Before the SEM observation, the samples were completely dried and coated with a thin layer of gold. The element mapping was carried out using the Elemental Analyzer Vario EL. XRD of the samples was performed using a Rigaku D/Max-2400 diffractometer with Cu K $\alpha$  radiation ( $k=1.5418 \text{ \AA}$ ) at 40 kV, 100 mA, and scanning from  $3^\circ$  to  $80^\circ$  at  $5^\circ/\text{min}$ . The thermograms have been recorded on a TGA-Q100 thermal analyzer at a temperature range from 0 to  $800^\circ\text{C}$  and with a heating rate of  $5^\circ\text{C min}^{-1}$  in an atmosphere of nitrogen.

### 3 Results and Discussion

#### 3.1 FTIR Analysis

On comparison with the FTIR spectra (Fig. 2) of XG, laterite, and XG-g-AA/laterite, the following results were obtained: (i) the sharp peak centered at  $3620 \text{ cm}^{-1}$  ascribed to the stretching vibration of the surface  $-\text{OH}$  groups of laterite disappeared after the reaction; (ii) the absorption peaks at  $1631 \text{ cm}^{-1}$  (Fig. 1) and  $1620 \text{ cm}^{-1}$  (Fig. 1) ascribed to the bending vibration of  $-\text{OH}$  groups disappeared after the reaction, and the new absorption peaks at  $1614 \text{ cm}^{-1}$  appeared in the spectra of XG-g-AA/laterite. (iii) The absorption peaks at  $1446 \text{ cm}^{-1}$  (Fig. 2(a)) and  $1436 \text{ cm}^{-1}$  (Fig. 2(b)) attributed to the C–OH bending vibration disappeared after the reaction, and new peaks were observed at  $1411 \text{ cm}^{-1}$  and were attributed to the symmetric stretching vibration of  $-\text{COO}$  groups; and (iv) the strong absorption bands at  $1028 \text{ cm}^{-1}$  (Fig. 2(a)) ascribed to  $\equiv\text{SiO}-$  stretching of laterite obviously weakened after the reaction, and the positions of the peaks at  $3415$  and  $3473 \text{ cm}^{-1}$  observed in XG-g-AA/laterite were also close to that of XG. These observations reveal that AA had been grafted onto the XG backbone, and the laterite also participated in the grafting copolymerization reaction through its active silanol groups (Wang et al. 2008a, b; Gils et al. 2009).

To analyze the elemental distribution, the element mapping images of carbon, oxygen, aluminum, ferrum, and silicon were shown in Fig. 3. As can be seen, aluminum, ferrum, and silicon were distributed evenly in carbon and oxygen, which indicated that laterite particles have been distributed in XG-g-AA/laterite

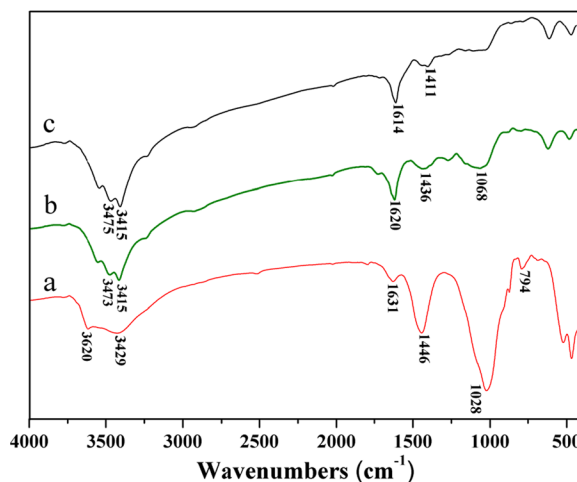


**Fig. 2** FTIR spectra of *a* laterite, *b* XG, and *d* XG-g-PAA/laterite

evenly because the major ingredients of laterite are aluminum, ferrum, and silicon.

#### 3.2 XRD Analysis

X-ray diffraction spectra of both laterite and XG-g-PAA/laterite were presented in Fig. 4. Laterite was a natural sample, and full identification of crystals was limited because of impurities and the possible presence of amorphous phases. The peaks at  $2\theta$  of 20.84, 26.62, 50.12, and 59.92 were associated with quartz as a major crystalline structure according to the standard powder diffraction data (PDF 65-0466). Also, the XRD peaks at  $2\theta$  of 8.78, 19.78, 34.98, and 61.66 were related to the calcite phase (PDF 05-0586). Furthermore, the XRD peaks at  $2\theta$  of 23.02, 29.42, 36.54, 39.46, 43.2, 47.54, and 48.58 were relevant to the muscovite phase (PDF 07-0042). In the case of XG-g-PAA/laterite composite, the weak broad peaks at  $2\theta$  of 21.58 were attributed to its amorphous structure of hydrogel with low crystallinity, and the diffraction peaks related to laterite disappeared or weakened, which is an indication of an exfoliated structure (Rashidzadeh and Olad 2014). In exfoliated structures, no more diffraction peaks were visible in the XRD diffractograms either due to a slight collapse of the plates that took place during the reaction, which led to the interlayer spacing reduction, or the structure of XG-g-PAA/laterite composite appeared to be partially exfoliated (Irani et al. 2014). The extensive layer separation associated with exfoliated structures disrupted the coherent layer stacking and resulted in a featureless diffraction pattern (Rashidzadeh and Olad 2014). From

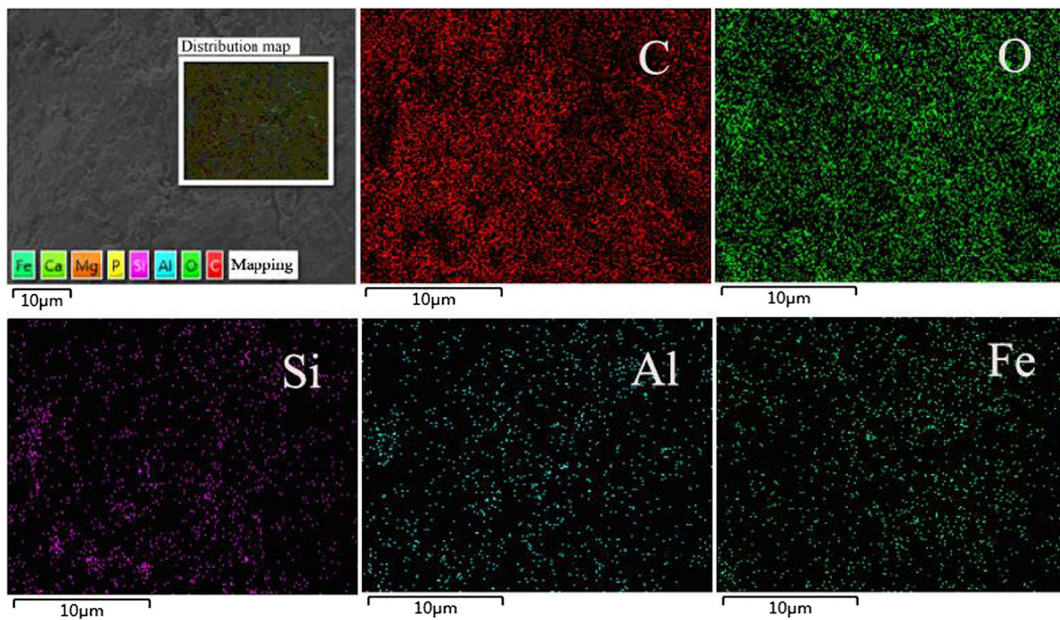


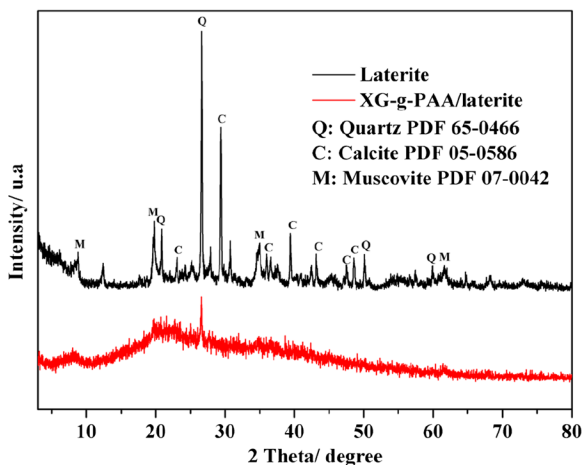
**Fig. 3** Element mapping of the NaAlg-g-PAA/organo-loess

the XRD results, it could be suggested that the polymer matrix should have interacted on the surface of laterite rather than being incorporated into the lamellae spacing.

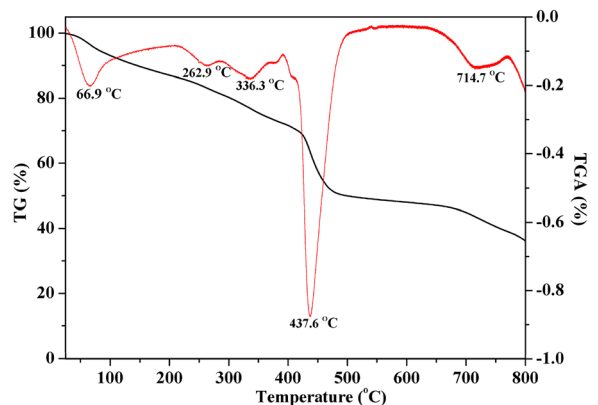
### 3.3 Thermogravimetric Analysis

Figure 5 shows TG and TGA curves of XG-g-PAA/laterite composite. The initial slight loss in weight was merely due to evaporation of the residual water in the composite. The second one in the interval of 217.1–288.6 °C had been ascribed to the dehydration and decarboxylation of the polymer which led to the

formation of inter- and intramolecular anhydride (Gils et al. 2009). The third stage of 288.6–390.9 °C might be due to elimination of CO<sub>2</sub> molecule from the polymeric backbone. The major weight loss of the polymer occurred in the fourth stage between 390.9 and 593.5 °C, and the  $T_{max}$  has been found at 437.6 °C. This was assigned to the elimination of the water molecule from the two neighboring carboxylic groups of the polymer chains with the formation of anhydride, main chain decomposition of the PAA, and destruction of the cross-linked network structure (Bao et al. 2011). The last stage that occurred at 714.7 °C might have been an acceptable evidence for the further decomposition or



**Fig. 4** XRD patterns for laterite and XG-g-PAA/laterite



**Fig. 5** TG/TGA curves of XG-g-PAA/laterite

degradation of residual organic matter at high temperatures (Zhang et al. 2014).

### 3.4 Morphological Studies

SEM microphotographs of laterite and sand particles and the fracture surface of the sand fixation specimen with different magnifications are presented in Fig. 6. It could be observed that laterite samples displayed a multilayer structure and nanosheets, and the distance between sheets is in nanoscales, which provides great surface reaction. Meanwhile, no flocculation of laterite nanosheets could be observed in the fracture surface of the sand fixation specimen, which indicated that laterite nanosheets were finely dispersed in the polymer matrix to form a homogeneous composition. For untreated sand particles, the transition zone around sand particles was more open and isolated from each other, containing more gaps of sand particles, and thus, was accompanied by a low compressive strength, which can be attributed to wind erosion and the collision of the sand particles in movement. By contrast, it was found that the sand fixation specimens containing CSFA showed a dense contact in the sand-sand particle transition zone, and the sand particles were bonded with each other through the CSFA, forming a bonding layer, which could increase compressive strength and hinder the movement of sand

particles to prevent wind erosion effectively. In addition, the bonding layer could prevent moisture evaporation to increase the water retention property of sand particles.

### 3.5 Influence of the Content of CSFA on Sand-Fixing Effect

In the desert environment, there are strong winds and large sandstorms that are severely destructive for the sand-fixing layer frequently. Therefore, it is necessary for the sand fixation specimens to have excellent compressive strength for wind erosion resistance. To determine the compressive strength of the sand fixation specimens, the specimens that contained different contents of CSFA, ranging from 0.4 to 2 %, were evaluated (Fig. 7). It could be seen that the compressive strength of the specimens was increased by increasing the content of the CSFA. When the content of the CSFA was increased from 0.4 to 2 %, the compressive strength was increased from 0.39 to 2.18 MPa, respectively. This could be explained that when the CSFA was added to the sand particles and formed a homogeneous mixture, a part of CSFA filled up the sand-sand particle transition zone, and the other part covered the surface of the sand particles. Meanwhile, when the content of CSFA was increased, the solidification of the molecular weight of the sand-fixing specimens increased, the cross-linking

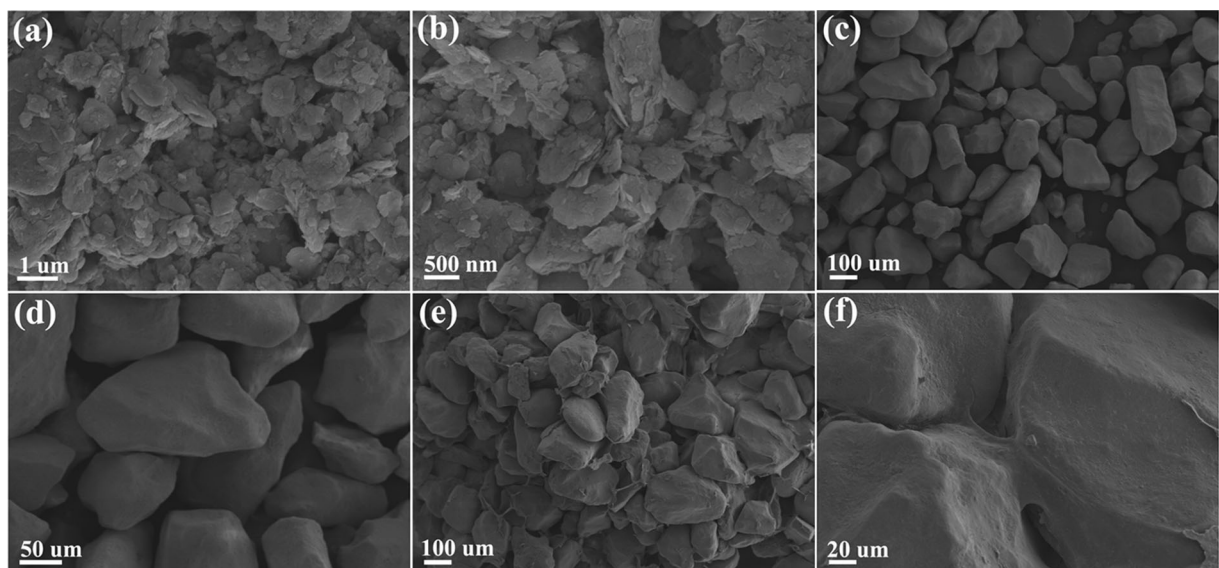


**Fig. 6** SEM micrographs of cross-sectional structure of **a, b** laterite and the sand fixation specimens: **c, d** without CSFA and **e, f** with 2 % CSFA (based on sand weight)

density increased, the electrostatic interactions (Coulombic and van der Waals) between groups on the chain increased, so the interaction force between the CSFA and sand particle increased (Yang et al. 2009). However, it was worth pointing out that the compressive strength of the sand fixation specimens containing 1.2 % sand-fixing agent was still higher than that of international standard requirements for a compressive strength of 1 MPa, and it could satisfy the practical application of sand fixation.

### 3.6 Water Resistance of the Specimens

Water resistance is also an important parameter that is used to assess the sand-fixing effect. As shown in Fig. 8, after the sand fixation specimens were immersed in water for 8 days, the specimen containing 0.4 wt% CSFA (Fig. 8a) became larger in volume due to absorption of water and surface cracks appeared. But for the specimen containing 0.8 wt% CSFA (Fig. 8b), there were no obvious surface cracks and the specimen containing 1.6 wt% CSFA (Fig. 8c) appeared to have slight surface cracks as well as the volume became larger after absorption of water. Meanwhile, it could not be observed that the sand particles fall out from the above specimens, which meant that the CSFA has certain water resistance. However, no obvious volume change and surface cracks could be observed in all the sand-fixing specimens (Fig. 8d–f) treated with  $\text{CaCl}_2$  solution. This phenomenon may be attributed to the existence of a large number of carboxyl in CSFA, and after immersion in  $\text{CaCl}_2$  solution, the network structure of  $\text{Ca}^{2+}$

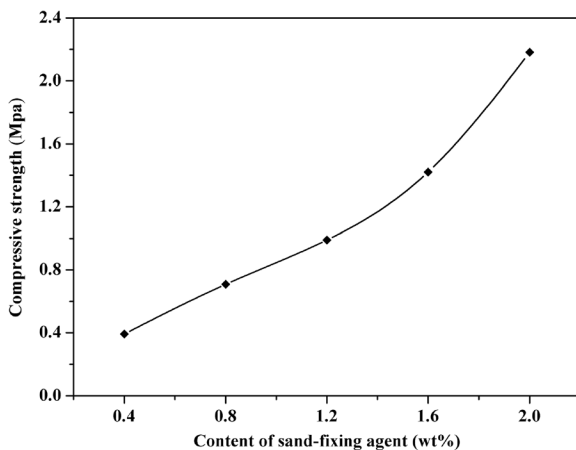


**Fig. 7** Relationship between the content of sand-fixing agent and the compressive strength

crosslinked formed on its surface (Mahdavinia et al. 2004), which improved the water resistance greatly.

Figure 9 presented the flexibility of the specimens which have been treated with  $\text{CaCl}_2$  solution and immersed in tap water for 8 days. It could be seen that all the specimens have certain flexibility, and more specifically, the flexibility was increased with the content of CSFA increased. This result might be an evidence for the fact that  $\text{Ca}^{2+}$  has improved the water resistance of the specimens and indicated that it could be used for practical application of sand fixation.

### 3.7 Influence of Thermal Aging on Sand-Fixing Effect

The effect of thermal aging on the compressive strength of the sand fixation specimens with different contents of CSFA (1.2 and 2 %, based on the weight of dry sand) is presented in Fig. 10. It can be observed that the specimens' compressive strength increased in the early stage of the thermal aging and then decreased continuously in the subsequent thermal aging test. This phenomenon might be due to the fact that there was an increase in the cross-linking density of the polymer in the early stage of the thermal aging test and, therefore, an initial increase in the compressive strength of the specimens. However, in the subsequent test, the continuous decrease in the compressive strength of the specimens was mainly caused by the degradation of the polymer molecules under the action of thermal aging (Yang et al. 2007a). But it is worth mentioning that there is no sharp decrease in the compressive strength with the increase of thermal aging time, which indicated that the sand-fixing agent exhibits an excellent thermal stability.

### 3.8 Influence of Freeze-Thaw Aging on Sand-Fixing Effect

Considering sand-fixing agent application in desert areas with a large temperature difference between day and night, the influence of freeze-thaw aging on sand-fixing effect was tested and the results are indicated in Fig. 11. It could be observed that there is a systematic decrease in the compressive strength of the specimens with increasing freeze-thaw aging cycles. The decrease of compressive strength might be attributed to the crack on the surface of the specimen brought by continuation of the freeze-thaw cycles (Yang et al. 2007a). Although the compressive strength decreased significantly when the number of freeze-thaw cycles increased, the



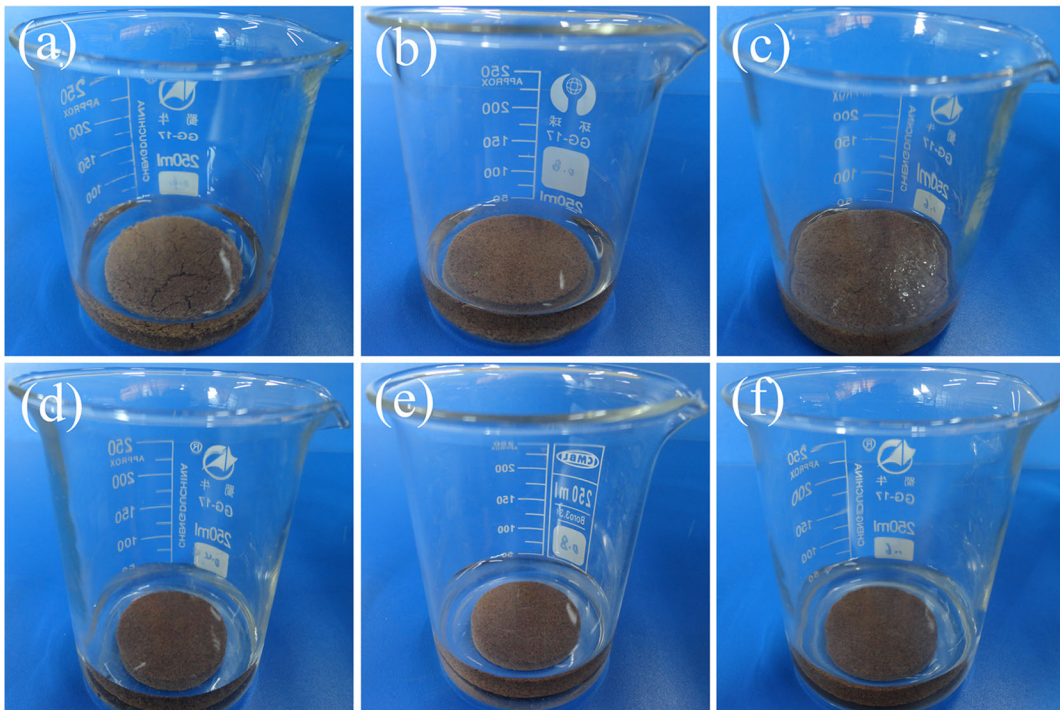


**Fig. 8** Water resistance of the sand fixation specimens containing different amounts of CSFA (a 0.4 %, b 0.8 %, c 1.6 %) and specimens (d 0.4 %, e 0.8 %, f 1.6 %) treated with the 10 wt%  $\text{CaCl}_2$  solution

compressive strength of the specimen containing 2 % CSFA still exceeded 1.84 MPa after 24 freeze-thaw aging cycles, which indicated that the sand-fixing agent showed a good freeze-thaw stability and could resist the great changes of temperature.

### 3.9 Influence of UV Radiation Aging on Sand-Fixing Effect

In the harsh desert environment, the sand-fixing agent exposed to air is extremely vulnerable to damage, and especially under high-intensity UV radiation, it could be decomposed. Therefore, the durability of the sand

fixation specimens under UV radiation is an important property for evaluating the sand-fixing agent. Figure 12 shows the variations of the different contents of CSFA with exposure time for the compressive strength of the specimen. It is clearly observed that the compressive strength of the specimen increased after 90–110 h of radiation and then decreased in the subsequent test. This phenomenon could be due to two simultaneous reactions: chain fracture and cross-linking reaction. The early occurrence of the cross-linking reaction dominates the chain fracture processes of degradation. When the radiation dose is excessive, more chains begin to be fractured, there are macromolecular changes to the

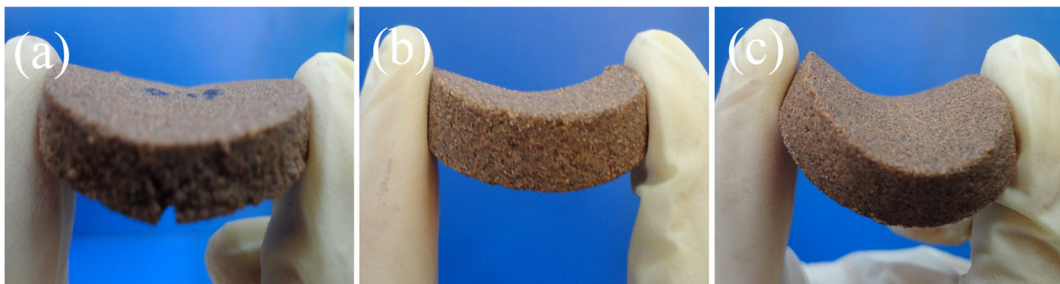


**Fig. 9** The flexibility of specimens containing different amounts of CSFA (a 0.4 %, b 0.8 %, c 1.6 %) treated with  $\text{CaCl}_2$  solution and immersed in tap water for 8 days

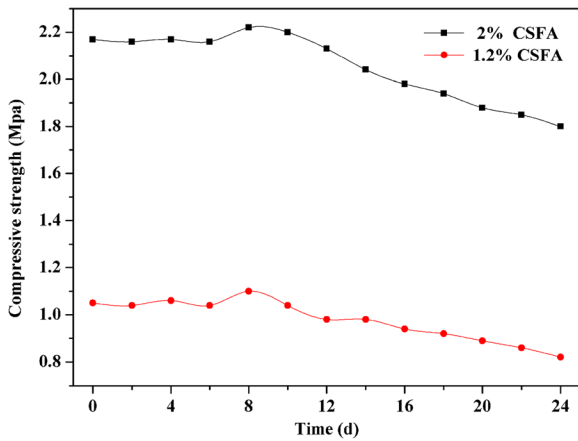


**Fig. 10** Relationship between the time and the compressive strength in thermal aging test

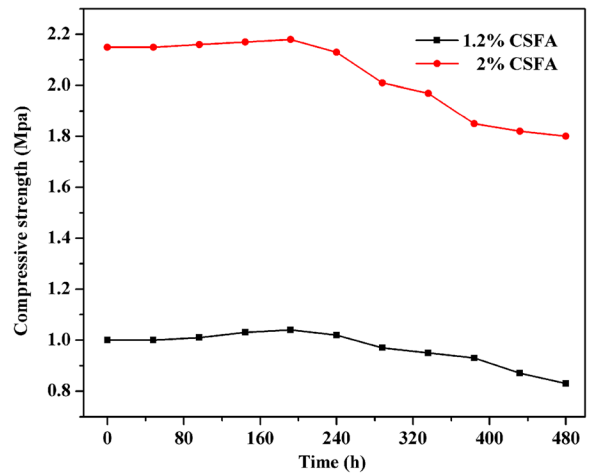


**Fig. 12** Relationship between the time and the compressive strength in UV radiation aging test

smaller one, and the polymer may lose its compressive strength (Yang et al. 2007b). However, after 480 h of continuous high-intensity UV radiation, the compressive strength of the specimens containing 2 % CSFA still exceeded 1.80 MPa. This result indicated that the sand fixation material has a good anti-ultraviolet aging performance and could meet the requirement of application in the field.

### 3.10 Water-Retaining Property of Sand Fixation Specimens

In arid and rainless desert areas, the survival rate of vegetation is very low because moisture evaporates quickly under the high-temperature environment.

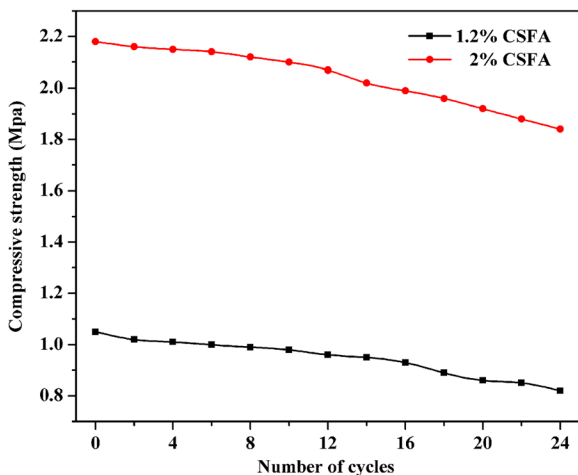


**Fig. 11** Relationship between the number of cycle and the compressive strength in freeze-thaw aging test

Therefore, the water-retaining property is an important parameter used to evaluate the effectiveness of sand-fixing agents in the relatively arid and desert areas. The relationship curves of the water-retaining property and drying time of the specimens which were treated with different amounts of CSFA are shown in Fig. 13. As observed, the water-retaining property of the treated specimens was more than that of the control through the same drying time. After 7 days, the specimen containing 0 % CSFA had no water. However, the water-retaining property of the specimen containing 2 % CSFA is still more than 40 %. These results indicated that the presence of CSFA improved the water-retaining property of sand obviously and it could be used as potential materials for sand fixation applications.

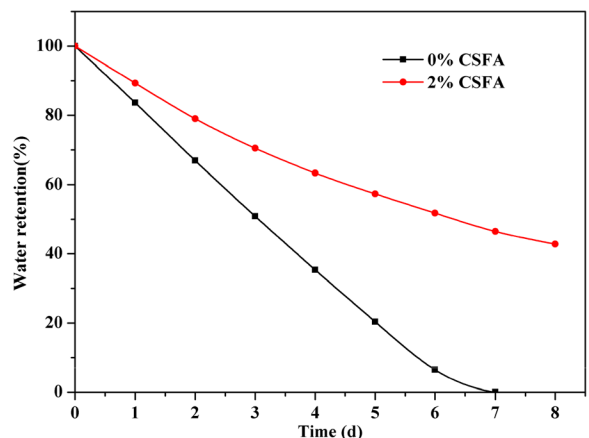


**Fig. 13** Relationship between the sand water content and evaporating time under 25 °C

## 4 Conclusions

In the present study, a novel, cost-effective, and eco-friendly chemical sand-fixing agent (XG-g-PAA/laterite) by means of graft copolymerization of XG, partially neutralized acrylic acid (NaA), and natural laterite was prepared. The results proved that the compressive strength of the specimens was increased by increasing the content of CSFA, and the addition of a low content of CSFA could obtain desired sand-fixing properties. Meanwhile, the chemical sand-fixing agent exhibited remarkable performances including water resistance, heat resistance, anti-freeze-thaw, and anti-ultraviolet aging, which indicated that the CSFA could meet the requirement of application in the harsh desert environment. In addition, it also showed excellent water-retaining and anti-evaporation properties. Considering the low cost and eco-friendliness of XG-g-PAA/laterite, we believed that it could be potential materials for sand-fixing applications to improve the efficiency of desert restoration.

**Acknowledgments** We thank the National Science Foundation of China (21164009) and the Ministry of Education Changjiang Scholars and Innovative Research Team (IRT1177) for financial support as well as the Key Laboratory of Eco-Environment-Related Polymer Materials (Northwest Normal University) of the Ministry of Education and the Key Laboratory of Polymer Materials of Gansu Province.

## References

- Asi, I. M., Al-Abdul Wahhab, H. I., Baghabra Al-Amoudi, O. S., Khan, M. I., & Siddiqi, Z. (2002). Stabilization of dune sand using foamed asphalt. *ASTM Geotechnical Testing Journal*, *25*(2), 168–176.
- Asner, G. P., & Martin, R. E. (2004). Biogeochemistry of desertification and woody encroachment in grazing systems. *Ecosystems and land use change*, 99–116.
- Bao, Y., Ma, J., & Li, N. (2011). Synthesis and swelling behaviors of sodium carboxymethyl cellulose-g-poly (AA-co-AM-co-AMPS)/MMT superabsorbent hydrogel. *Carbohydrate Polymers*, *84*(1), 76–82.
- Dong, G., Chen, H., Wang, G., Li, X., Shao, Y., & Jin, J. (1995). Evolution of deserts and sandy lands of northern China and its relationships with climate change over the past 150 ka. *Science in China Series D: Earth Sciences*, *25*, 1303–1312 (in Chinese).
- Dong, Z., Wang, L., & Zhao, S. (2008). A potential compound for sand fixation synthesized from the effluent of pulp and paper mills. *Journal of Arid Environments*, *72*(7), 1388–1393.
- Duan, J., Litwiller, E., Choi, S. H., & Pinnau, I. (2014). Evaluation of sodium lignin sulfonate as draw solute in forward osmosis for desert restoration. *Journal of Membrane Science*, *453*, 463–470.
- Eldridge, D. J., & Ferris, J. M. (1999). Recovery of populations of the soil lichen *Psora crenata* after disturbance in arid South Australia. *Rangeland Journal*, *21*(2), 194–198.
- Gils, P. S., Ray, D., & Sahoo, P. K. (2009). Characteristics of xanthan gum-based biodegradable superporous hydrogel. *International Journal of Biological Macromolecules*, *45*(4), 364–371.
- Hashemimaneh, M., & Matinfar, H. (2012). Evaluation of desert management and rehabilitation by petroleum mulch base on temporal spectral analysis and field study (case study: Ahvaz, Iran). *Ecological Engineering*, *46*, 68–74.
- Hua, T., Wang, X., Lang, L., & Zhang, C. (2014). Variations in tree-ring width indices over the past three centuries and their associations with sandy desertification cycles in East Asia. *Journal of Arid Environments*, *100*, 93–99.
- Irani, M., Ismail, H., & Ahmad, Z. (2014). Hydrogel composites based on linear low-density polyethylene-g-poly (acrylic acid)/kaolin or halloysite nanotubes. *Journal of Applied Polymer Science*, *131*(8). doi:10.1002/APP.40101.
- Ji, S., & Unger, P. W. (2001). Soil water accumulation under different precipitation, potential evaporation, and straw mulch conditions. *Soil Science Society of America Journal*, *65*(2), 442–448.
- Jiang, Z., Lian, Y., & Qin, X. (2014). Rocky desertification in southwest China: impacts, causes, and restoration. *Earth-Science Reviews*, *132*, 1–12.
- Li, X. Y., Gong, J. D., & Wei, X. H. (2000). In-situ rainwater harvesting and gravel mulch combination for corn production in the dry semi-arid region of China. *Journal of Arid Environments*, *46*(4), 371–382.
- Liu, J., Shi, B., Lu, Y., Jiang, H., Huang, H., Wang, G., & Kamai, T. (2012). Effectiveness of a new organic polymer sand-fixing agent on sand fixation. *Environmental Earth Sciences*, *65*(3), 589–595.
- Mahdavinia, G. R., Pourjavadi, A., Hosseinzadeh, H., & Zohuriaan, M. J. (2004). Modified chitosan 4. Superabsorbent hydrogels from poly (acrylic acid-co-acrylamide) grafted chitosan with salt- and pH-responsiveness properties. *European Polymer Journal*, *40*(7), 1399–1407.
- Mazor, G., Kidron, G. J., Vonshak, A., & Abeliovich, A. (1996). The role of cyanobacterial exopolysaccharides in structuring desert microbial crusts. *FEMS Microbiology Ecology*, *21*(2), 121–130.
- Musa, A., Deming, J., & Cunyang, N. (2014). The applicable density of sand-fixing shrub plantation in Horqin Sand Land of northeastern China. *Ecological Engineering*, *64*, 250–254.
- Rashidzadeh, A., & Olad, A. (2014). Slow-released NPK fertilizer encapsulated by NaAlg-g-poly (AA-co-AAm)/MMT superabsorbent nanocomposite. *Carbohydrate Polymers*, *114*, 269–278.
- Wang, S. Y., & Dong, J. B. (2001). The rise and fall of Tongwan city with the environmental change of Mu Us sandy land. *Geography Research*, *20*, 347–353 (in Chinese).
- Wang, T., Zhu, Z., & Wu, W. (2002). Sandy desertification in the north of China. *Science in China Series D: Earth Sciences*, *45*(1), 23–34.

- Wang, X., Chen, F., Hasi, E., & Li, J. (2008a). Desertification in China: an assessment. *Earth-Science Reviews*, 88(3), 188–206.
- Wang, W., Zheng, Y., & Wang, A. (2008b). Syntheses and properties of superabsorbent composites based on natural guar gum and attapulgit. *Polymers for Advanced Technologies*, 19(12), 1852–1859.
- Wang, X., Chen, F., Zhang, J., Yang, Y., Li, J., Hasi, E., & Xia, D. (2010). Climate, desertification, and the rise and collapse of China's historical dynasties. *Human Ecology*, 38(1), 157–172.
- Yang, J., Wang, F., Fang, L., & Tan, T. (2007a). The effects of aging tests on a novel chemical sand-fixing agent—polyaspartic acid. *Composites Science and Technology*, 67(10), 2160–2164.
- Yang, J., Wang, F., Fang, L., & Tan, T. (2007b). Synthesis, characterization and application of a novel chemical sand-fixing agent-poly (aspartic acid) and its composites. *Environmental Pollution*, 149(1), 125–130.
- Yang, J., Wang, F., & Tan, T. (2009). Controlling degradation and physical properties of chemical sand fixing agent-poly (aspartic acid) by crosslinking density and composites. *Journal of Applied Polymer Science*, 111(3), 1557–1563.
- Zhang, M., Cheng, Z., Liu, M., Zhang, Y., Hu, M., & Li, J. (2014). Synthesis and properties of a superabsorbent from an ultraviolet-irradiated waste nameko mushroom substrate and poly (acrylic acid). *Journal of Applied Polymer Science*, 131(13). doi:10.1002/app.40471.
- Zhou, W., Gang, C., Zhou, F., Li, J., Dong, X., & Zhao, C. (2015). Quantitative assessment of the individual contribution of climate and human factors to desertification in northwest China using net primary productivity as an indicator. *Ecological Indicators*, 48, 560–569.